

Cholesteric Liquid-Crystal Copolyester, Poly[oxycarbonyl-1,4-phenylene-oxy - 1,4 terephthaloyl-oxy- 1,4-phenylene-carbonyloxy (1,2-dodecane)] $[C_{34}H_{36}O_8]_n$, Synthesized from Racemic Materials: Kinetics, Structure and Optical Characterization.

Mercedes Pérez Méndez *, Javier Sanguino Otero *

*Institute of Polymer Science and Technology, CSIC, Group of Physical-Chemistry and Modelization of Macromolecules (PCMM), C/ Juan de la Cierva, 3. 28006 Madrid, Spain.

ABSTRACT

The cholesteric liquid-crystal poly[oxycarbonyl-1,4-phenylene-oxy-1,4 terephthaloyl-oxy-1,4-phenylene-carbonyloxy(1,2-dodecane)] $[C_{34}H_{36}O_8]_n$, named PTOBDME, synthesized by polycondensation reaction from equimolar quantities of TOBC and the *racemic* mixture of glycol (R-S-1,2 dodecanediol), exhibits unexpected optical activity and chiral morphology. The structure of *racemic*-PTOBDME, under different polymerization kinetics conditions, is analyzed by conventional NMR techniques and compared with those of polymer enantiomers R-PTOBDME and S-PTOBDME obtained starting R(+),1,2 and S(-),1,2-dodecanediol respectively. Molecular models based on the NMR signals intensities are proposed. The optical activity of *racemic*-PTOBDME is evaluated by measuring the ORD values during kinetics study, and compared to the chiral polymers. Each enantiomeric polymer seems to present the same stereoregular head-tail, isotactic structure than the *racemic*, which we explain by the higher reactivity of the primary hydroxyl than the secondary one in the glycol through polycondensation. For each enantiomer, two independent sets of signals were observed by NMR, explained as two diastereomeric helical conformers: *gg* and *gt*, related with two possible staggered conformations, along the copolymer backbone. Chirality in *racemic*-PTOBDME is proposed to be due to the kinetic resolution of a preferable helical diastereomer, such as *Sgt*, with respect to the possible four forms, while the R/S ratio of asymmetric carbon atoms remained 50:50. Chiral amplification is observed in R-PTOBDME and S-PTOBDME due to a helical screw sense excess. Optimum yield was obtained for *racemic* PTOBDME, after 120 minutes polycondensated and decanted in toluene for 24 hours. Two weeks later a second fraction precipitated from the toluene mother liquor with 67.6% chiral excess. After eight months and two weeks a third fraction precipitated with 85.2% chiral excess.

Keywords: Cholesteric LC-polymer, crystal modelling, kinetics, optical activity.

I. INTRODUCTION

There is a growing interest in the development of optically active synthetic polymers and their structure control. Three major groupings can be established: polymers with optical activity arising from asymmetric centers in the side or main chain; polymers with optical activity arising from both asymmetric centers and macromolecular asymmetry based on the secondary structure (i.e., a helix), and polymers with optical activity arising entirely from macromolecular asymmetry [1].

Polymeric liquid crystals have a mesophase state in a temperature range between those of crystal formation and the melt, combining order of crystals with mobility of liquids. The parallel orientation of their longitudinal molecular axes is common to all mesophases (long-range-order) [2]. Two major classes can be distinguished: *nematic* (with

molecular centres distributed isotropically) and *smectic* (molecular centres organized in layers). The special array of nematic planes stacked in a helical superstructure with a prevalent screw direction is called *cholesteric* mesophase - twisted nematic.

Cholesteric liquid crystal polyester $[C_{34}H_{36}O_8]_n$, named PTOBDME for the research described here, was obtained by polycondensation reaction between 4,4'-(terephthaloyl-di(oxybenzoic) chloride (TOBC) and R-S-1,2 dodecanediol, followed by decantation in toluene [3], according to the method previously reported by Bilibin [4, 5]. The chemical repeat unit, in Fig. 1, exhibits amphiphilic character, with an hydrophilic rigid core - mesogenic group- along the main chain, with three benzene rings bonded by ester bridges, and an hydrophobic- flexible aliphatic side chain, both linked by a spacer.

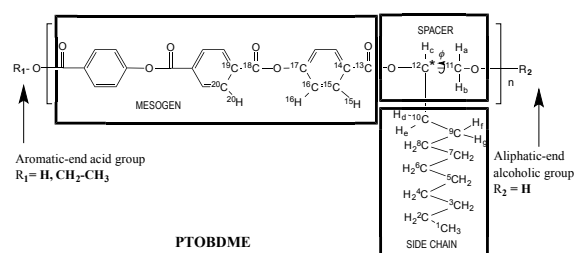


Figure 1. Monomeric unit of cholesteric liquid crystalline PTOBDME. The three different zones of the monomer: mesogen, spacer and flexible side chain are indicated. Hydrogen and carbon atoms have been numbered as previously reported [6]. The asterisk indicates the chiral center (^{12}C). Torsion ϕ , along ^{11}C - ^{12}C bond, is indicated. Aromatic-end acid and aliphatic-end alcoholic groups are also specified.

Although only racemic materials were used in the synthesis, a cholesteric, chiral morphology, theoretically not expected, was found, see Fig.2. Evidence of this was obtained when a white solid, recrystallized, as the second fraction, from toluene mother liquor after the filtration of the polymer, was identified as -PTOBDME, with $[\alpha]_{589}^{25} = -1.43$ [1.538 gr/100ml, toluene] [6]. A similar result had been previously obtained for the liquid crystal PTOBEE, $[\text{C}_{26}\text{H}_{20}\text{O}_8]_n$, also obtained as cholesteric, from polycondensation reaction between the racemic glycol R-S-1,2-butanediol and TOBC [7], with a similar molecular formula as PTOBDME except the side chain is an ethyl group instead of decanyl. Its second fraction was isolated as -PTOBDME, with a value of $[\alpha]_{589}^{25} = -2.33$ [0.0056 mol/l, toluene]. Its structure and diastereomeric excess were characterized by NMR [8].

Repeat unit models were simulated for PTOBDME by Molecular Mechanics calculations with Materials Studio, Fig. 3(a). The conformers with lower energy always “polymerized” in macromolecules showing helical conformation along the main chain.

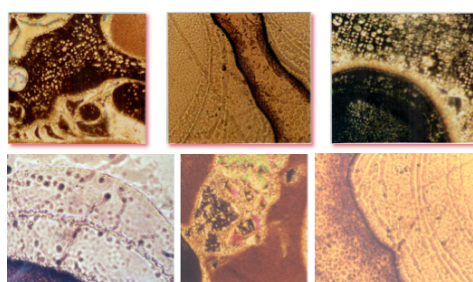


Figure 2. Cholesteric morphology of PTOBDME.

The simulated helical macromolecules could be packed, into a triclinic primitive P1 unit cell, oriented parallel to the c axis, with parameters: $a=5.5\text{\AA}$, $b=4.7\text{\AA}$, $c=111.2\text{\AA}$ (equal to the pitch length of the simulated polymer helix), $\alpha=92^\circ$, $\beta=112^\circ$, and $\gamma=90^\circ$ [6], Fig. 3(b).

From the polymer crystal model, theoretical powder x-ray diffraction patterns could be recalculated that matched the experimental one, confirming the model. The crystal morphology could further be simulated. The rhombohedral shape of “theoretical crystals” (pink in Fig. 3b) perpendicular to the c axis was in good agreement with the two single crystals types of each enantiomeric component, obtained dispersed within the mesophase matrix, after heated to mesophase and cooled, between two microscope glass plates, Fig. 3(c).

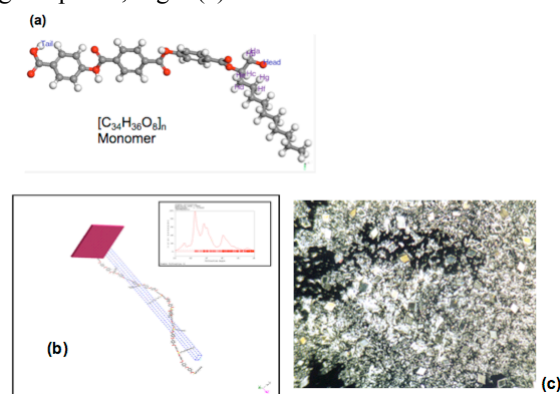


Figure 3. (a) MM model of PTOBDME repeat unit; (b) Crystal packing simulation of PTOBDME. Recalculated WAXS on the upper right hand corner and morphology simulation from crystal model; (c) Optical micrograph of single crystals of PTOBDME spontaneously grown in two rhombohedral families, dispersed in mesophase matrix.

PTOBDME behaves both as thermotropic and lyotropic, which confers on it interesting macromolecular properties in the field of biotechnology [9, 10, 11].

In the present paper we report a deeper study on the PTOBDME polymerization reaction, starting from *racemic* 1,2 dodecanediol, establishing the best yield under different kinetics conditions, and compare it with R-PTOBDME and S-PTOBDME obtained by polycondensation reaction between TOBC and R(+) and S(-)-1,2-dodecanediol, respectively.

The helical structure of PTOBDME is determined in solution by NMR with the complete assignment of ^1H and ^{13}C signals together with the polymer conformational analysis. Polymer chirality is evaluated by optical rotatory dispersion (ORD). The relationship between ORD values and conformations given by the NMR spectra is established for *racemic* and chiral PTOBDME.

II. MATERIALS AND METHODS

2.1. Synthesis of cholesteric *racemic* PTOBDME and *chiral* R-PTOBDME and S-PTOBDME.

The synthesis of PTOBDME, already described elsewhere [3], [6], was carried out by polycondensation of equimolar quantities of 4,4'-(terephthaloyldioxydibenzoic chloride) (TOBC) and

a racemic mixture of R-S-1,2-dodecanediol from Fluka Chemie GmbH (Switzerland), dissolved in diphenyl oxide in N₂ atmosphere. The dichloride, TOBC, was obtained by reaction between thionyl chloride and 4,4'-(terephthaloyldioxydibenzoic) acid (TOBA), previously synthesized from terephthaloyl chloride and 4-hydroxybenzoic acid.

Pure enantiomeric R(+)-1,2-dodecanediol and S(-)-1,2-dodecanediol, purchased from Sigma-Aldrich (Spain), were used instead to produce R-PTOBDME and S-PTOBDM respectively.

Surveyed kinetics variables were: Time of polycondensation reaction, stirring rate, time of polymer decantation in toluene, time at which the second and even third polymer fractions were precipitated and yields.

2.2. Characterization Techniques

Conventional NMR techniques: ¹H-NMR, ¹³C-NMR, TOCSY (Total correlation spectroscopy), COSY (Homonuclear correlation spectroscopy) and HSQC (Heteronuclear single-quantum correlation spectroscopy), were used at room temperature, in a Varian SYSTEM 400 MHz spectrometer (Agilent, USA), using DMSO-d₆ from Merck KGaA (Germany) as solvent. NOESY (Nuclear Overhauser effect spectroscopy, through-space correlation method), ROESY (Rotating frame nuclear Overhauser effect spectroscopy) and DOSY (Diffusion ordered spectroscopy) were performed in a BRUKER 500 MHz spectrometer.

¹H chemical shifts were referenced to the residual solvent signal at δ = 2.50 ppm (DMSO-d₆) relative to tetramethylsilane (TMS). All the spectra were processed and analyzed with Mestrec 4.1.1 software [12].

Optical rotatory dispersion (ORD) was registered at 25°C in DMSO from Scharlau Chemie (Germany), in a Perkin-Elmer polarimeter 241MC (USA), E = 40 μA, with λ_{Na} = 589 nm, slit = 5 mm; λ_{Hg} = 574 nm, slit = 14 mm; λ_{Hg} = 546 nm, slit = 30 mm; λ_{Hg} = 435 nm, slit = 5 mm; λ_{Hg} = 365 nm, slit = 2.5 mm. Integration time was 50 s in all cases.

The molecular modelling work was performed with the software Materials Studio version 8.0 supplied by DS BIOVIA, Cambridge, U.K.

III. RESULTS AND DISCUSSION.

3.1. Structural analysis of PTOBDME in solution by NMR.

The ¹H-NMR and ¹³C-NMR spectra of PTOBDME are shown in Fig. 4 and Fig. 5, respectively.

The interpretation and assignment of signals for the PTOBDME polymer, the aliphatic-side end group and the aromatic-side acid end group, are presented in Table 1, considering ¹H-NMR, ¹³C-NMR, TOCSY, COSY, HMQC and HSQC experiments, together with the theoretical chemical shift values,

calculated with CS ChemNMR Pro versión 9.0 Scientific Software (R. Buerger Schaller, Upstream Solutions GmbH, Development Centre, Zurich, Switzerland).

The observed values can be compared with those of PTOBEE, with also two independent set of signals [8], and with analogous compounds with aliphatic end groups, as 2-hydroxydodecyl benzoate and 2-hydroxyalkyl benzoates [13-15].

The presence of chiral carbon atoms, ¹²C*, in the PTOBDME repeat unit promotes the presence of two enantiomers not distinguishable by NMR. Only diastereotopic H atoms attached to carbon atoms in α position to the chiral centre ¹²C* can be differentiated by splitting into two signals: In our case these are H_a and H_b attached to ¹¹C and H_d and H_e bonded to ¹⁰C. They exhibit coupling with each other and with the H_c atom directly bonded to chiral ¹²C*.

Besides chirality due to the asymmetrical carbon atom, there is a second chirality due to the helical conformation of PTOBDME, previously predicted and confirmed by Raman experiments [6], and by NMR for PTOBEE [8]. This implies two diastereomeric structures, for each enantiomeric polymer chain, i. e., four possible structures.

According to Ute *et al.* and Tabei *et al.* [16-19], when an isotactic polymer with asymmetric carbon atoms carries non-identical end-groups (R₁ ≠ R₂), each polymer can have two enantiomers, e.g., R₁, R, R, ..., R₂ and R₁, S, S, ..., R₂. The right-handed and left-handed helical conformations in each enantiomer, being diastereomeric structures whose energies differ from one another (ΔG ≠ 0), each helical state can be observed by NMR as an independent set of signals.

Hence, in PTOBDME the presence of the chiral carbon ¹²C* in the repeat unit, and the different end groups for the aliphatic-end (-OH) and aromatic-end (-COOH) promotes the presence of two enantiomers for an isotactic stereoregularity. Due to its helical-conformation, each enantiomer, R, R, R, and S, S, S, generates two different diastereomeric structures. In the NMR spectra, three sets of independent signals should be observed. Two are interpreted as caused by the helical conformations in the monomeric unit, differentiated with the apostrophe (') and without it (), and the third one, due to the aliphatic end-group unit, being indicated with double apostrophe ('').

The ¹H-NMR signals between 5.5 and 3.5 ppm were assigned to the polymer spacer, similar to those of PTOBEE, with analogous signals.

Observed at 5.45, 5.26, 4.64, 3.94 and 3.8 ppm, they are clues to conformational changes, much more affected by the effect of helicity than the rest of the protons in both diastereomers.

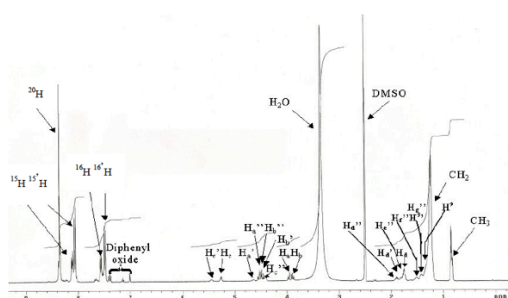


Figure 4. ¹H-NMR spectrum of PTOBDME. Signals with apostrophe (') and without it (blank) are attributed to two independent conformers of the repeating unit respectively (later called *gg* and *gt*). Signals (' ') on Table 1 are used to identify the aliphatic-end OH group. Peaks between 7- 7.36 ppm, are due to solvent impurities from the synthetic process.

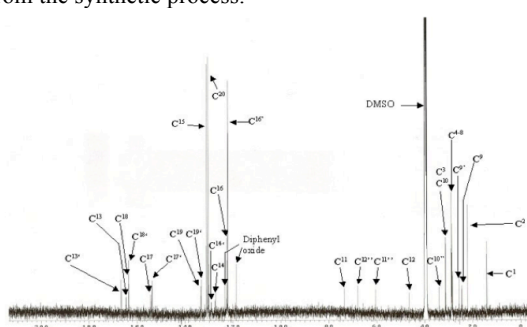


Figure 5. ¹³C-NMR spectrum of PTOBDME. Signals () and (') are attributed to two independent helical conformers. Signals (' ') correspond to the aliphatic end group, as in Fig. 4. Peaks at 118.6, 123.4 and 130.1 ppm, are due to diphenyl oxide impurities.

Accordingly, the multiplets at 5.45 and 5.26 ppm were assigned to H_{c'} and H_c respectively, attached to the asymmetric ¹²C* in each repeat unit of the two independent diastereomeric structures. The rest of the signals on Table 1, were correlated with H_{c'} or with H_c and assigned, respectively, to each of the two sets of chemical shifts with the symbol either (') or (). The H_{c'}: H_c integrals ratio, can be used to estimate the proportion between these two sets of signals.

The multiplet around 4.40 ppm, is interpreted as due to the proton attached to ¹²C* in the end spacer, hence called H_{c''}, similarly as it has been described in analogous compounds [13-15].

Diastereotopic protons H_a and H_b, bonded to ¹¹C (in α position with respect to asymmetric ¹²C*), split into double doublets centred at 3.94 and 3.88 ppm, respectively, with coupling constant $^3J_{(H_a-H_b)} = 11.7$ Hz; their integrals were in a ratio 1:1 and both signals together in a proportion 2:1 with respect to H_c.

The doublet at 4.64 ppm, with integral in a relation 1:1 to H_{c'}, belongs to H_{a'}.

The complex multiplet between 4.56 and 4.44 ppm is attributed to the overlapped signals of H_{b'} and H_{a''}H_{b''}. After subtraction of the H_{a'} integral value

(similar to H_{b'}), the remaining signal from 4.58 to 4.44 ppm, is interpreted as due to H_{a''} and H_{b''}, nearly double the integral of the signal at 4.40 ppm (H_{c''}).

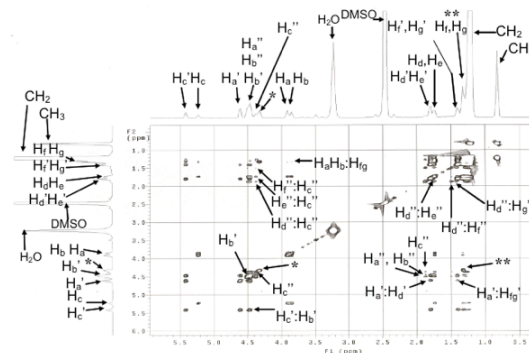


Figure 6. TOCSY Experiment of PTOBDME in the aliphatic zone, spacer and side chain.

(*) refers to methylene in the aromatic-side end group ph-COO-CH₂-CH₃ and (**) to methyl ph-COO-CH₂-CH₃.

The TOCSY 2D experiment, the results shown in Fig. 6, allowed us to observe correlations for each of the three independent aliphatic sets of ¹H signals. Hence, the H_c signal at 5.26 ppm was related with H_a (3.94 ppm), H_b (3.88 ppm), H_d, H_e (1.75 ppm), and H_f, H_g (1.33 ppm). The broad signal in Fig. 6, centered at 4.48 ppm, is interpreted as due to H_{b'}. It shows correlations with H_{a'} (4.64 ppm), H_{c'} (5.45 ppm), H_{d'}, H_{e'} (at 1.81 ppm) and H_{f'}, H_{g'} (at 1.42 ppm). At both sides of H_{b'}, two signals are interpreted as due to H_{a''} at (4.48 ppm) and H_{b''} at (4.49 ppm) respectively, forming part of the third system (' '), attributed to the aliphatic end group. The signal at 4.40 ppm (H_{c''}) presents correlations with H_{a''}, H_{b''} and H_{d''} at 1.89 ppm; H_{e''} at 1.75 ppm; H_{f''} at 1.51 ppm; H_{g''} at 1.42 ppm; and CH₂ centered at 1.22 ppm. Methylene and methyl protons of the aromatic ester end group, ph-COO-CH₂-CH₃, were also detected as CH₂ (4.32 ppm) quoted as * in Fig. 6 and Table 1, and as CH₃ (1.33 ppm) indicated as **.

The COSY H-H experiments provided interactions between coupled nuclei at a maximum three covalent bonds apart. They complemented the information obtained by TOCSY, and let us accurately assign the overlapped signals between 1.89-1.75 ppm and between 1.51-1.33 ppm as: H_{d''} 1.89 ppm; H_{d'} 1.81 ppm, H_{e''} 1.75 ppm and H_d 1.75 ppm, H_f and H_g 1.33 ppm and also H_{f'} 1.51 ppm; H_{g''} 1.42 ppm, H_{f'}, H_{g'} 1.42 ppm; and H_f, H_g 1.33 ppm.

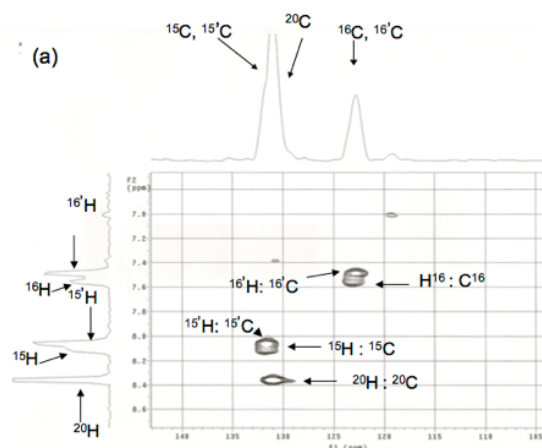


Figure 7(a). HSQC spectrum of PTOBDME in the aromatic zone.

In the aromatic zone, in Fig. 4, a singlet at 8.36 ppm was assigned to ^{20}H . Two doublets at 8.13 and 8.07 ppm, were assigned to ^{15}H and at 7.57 and 7.50 ppm to ^{16}H , in agreement with the model calculated with CS ChemNMR Pro versión 9.0 Scientific Software.

Since integral values of the doublets at 8.13 and 7.57 ppm increased with that of the H_c signal at 5.26 ppm, they were assigned to ^{15}H and ^{16}H , respectively. Similarly, integral values of doublets at 8.07 ppm and 7.50 ppm increased with that of H_c' (at 5.45 ppm); they were assigned to ^{15}H and ^{16}H . NOESY-2D experiment confirmed these correlations, as will be shown in Fig. 10.

Surprisingly the integral values due to ^{15}H and ^{16}H always remained in a larger proportion than those of ^{15}H and ^{16}H , perhaps due to the contribution of the final aromatic-COOH acid group, which overlapped in this zone. As was expected, crossing signals were observed in the TOCSY and COSY experiments between ^{16}H and ^{15}H but there was too much overlapping to distinguish the two systems.

The complete assignment of the chemical shifts, also in Table 1, was carried out with the help of the ^{13}C -NMR and the HSQC experiments. A detail of the HSQC spectrum of PTOBDME in the aromatic zone is displayed in Fig. 7(a).

Correlations between diastereotopic protons and their bonded carbon atoms in the spacer are seen in Fig. 7(c): H_c : 5.26 ppm with ^{12}C : 73.4 ppm; H_c' : 5.45 ppm with ^{12}C : 72.6 ppm; H_a : 4.64 ppm and H_b : 4.48 ppm with ^{11}C at 66.0 ppm; H_a, H_b at 3.94 and 3.88 ppm with ^{11}C at 46.4 ppm and $\text{H}_a''\text{H}_b''$ at 4.48 and 4.49 ppm with ^{11}C at 67.8 ppm.

Also correlations in the lateral chain of aliphatic end groups can be observed in Fig. 7(b) between signals: $\text{H}_d''\text{H}_e''$ at 1.89 and 1.75 ppm with ^{10}C at 34.5 ppm; and $\text{H}_f''\text{H}_g''$ at 1.51 and 1.42 ppm with ^9C at 26.5 ppm, respectively.

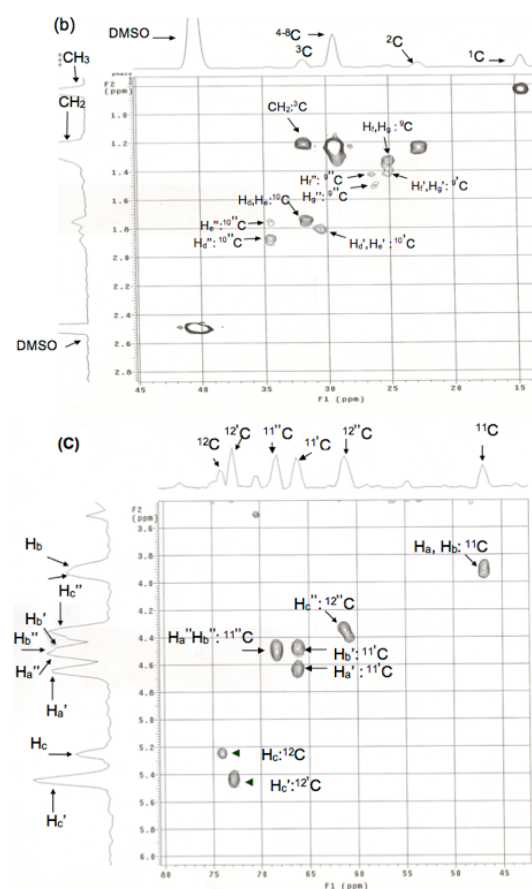


Figure 7(b). HSQC spectrum of PTOBDME in the lateral chain and in the spacer zone 7(c).

The chemical shifts of the quaternary carbon atoms, ^{14}C , ^{17}C , ^{19}C and carbonyl, ^{13}C , ^{18}C , observed in ^{13}C -NMR spectrum in Fig. 5, were assigned in agreement with the chemical shifts calculated with the CS ChemNMR Pro versión 9.0 Scientific Software, as shown in Table 1.

3.2. Structural analysis of R-PTOBDME and S-PTOBDME by NMR in solution.

^1H -NMR, ^{13}C -NMR, TOCSY, COSY and HSQC spectra were also obtained for R-PTOBDME and S-PTOBDME and compared to those of *racemic* PTOBDME. The same sets of chemical shifts observed for PTOBDME, synthesized from *racemic* DL:1,2-dodecanediol, were observed in the two chiral polymers obtained starting from pure enantiomeric glycols. R-PTOBDME and S-PTOBDME are isotactic polymers with enantiomeric structures: R-R-R-R... and S-S-S-S..., respectively. Due to their helical conformation, each one has two different diastereomeric structures, responsible for the two different independent sets of signals observed by NMR, since only diastereomers can be differentiated by this technique.

Table 1. ¹H and ¹³C-NMR Chemical Shifts (ppm) observed and calculated for the Chiral Polyester PTOBDME obtained from racemic 1,2-dodecanediol

Set of signal of gg helical conformer (↘)			Set of signal of gt helical conformer (↘)			Calculated Chemical Shifts		
Atom	¹ H ppm	¹³ C ppm	Atom	¹ H ppm	¹³ C ppm	Atom	¹ H ppm	¹³ C ppm
¹ H	8.36	¹³ C	¹³ C	130.4	¹ H	8.36	¹³ C	130.4
		¹³ C	133.2			¹³ C	133.2	135.5
		¹³ C	163.5			¹³ C	163.4	165.2
		¹³ C	153.9			¹³ C	154.4	155.7
¹ H	7.50;7.48	¹³ C	122.2	¹ H	7.57;7.55	¹³ C	122.5	7.26
¹ H	8.07;8.05	¹³ C	131.0	¹ H	8.13;8.11	¹³ C	131.0	8.13;8.11
		¹³ C	128.7			¹³ C	127.3	127.0
		¹³ C	166.6			¹³ C	164.5	166.0
H _c '	5.45	¹³ C	72.6	H _c	5.26	¹³ C	73.4	4.55
H _a 'H _b '	4.64; 4.48	¹³ C	66.0	H _a H _b	3.94; 3.88	¹³ C	46.4	4.80;4.55
H _a 'H _c '	1.81	¹³ C	30.3	H _a H _c	1.75	¹³ C	31.1	1.71
H _b 'H _c '	1.42	¹³ C	24.5	H _b H _c	1.33	¹³ C	24.5	1.29
¹ H	1.22	¹³ C	28.9(m)*	¹ H	1.22	¹³ C	28.9(m)*	1.29
¹ H	1.22	¹³ C	28.9(m)*	¹ H	1.22	¹³ C	28.9(m)*	1.29
¹ H	1.22	¹³ C	28.8(m)*	¹ H	1.22	¹³ C	28.8(m)*	1.26
¹ H	1.22	¹³ C	28.7(m)*	¹ H	1.22	¹³ C	28.7(m)*	1.26
¹ H	1.22	¹³ C	28.4(m)*	¹ H	1.22	¹³ C	28.4(m)*	1.26
¹ H	1.22	¹³ C	31.3	¹ H	1.22	¹³ C	31.3	1.26
¹ H	1.22	¹³ C	22.1	¹ H	1.22	¹³ C	22.1	1.26
¹ H	0.84	¹³ C	14.0	¹ H	0.84	¹³ C	14.0	0.86

Experimental aliphatic end group signals			Theoretical aliphatic end group signals				
H _c '	4.40	¹³ C	60.4	H _c '	3.81	¹³ C	70.9
H _a 'H _b '	4.48; 4.49	¹³ C	67.8	H _a 'H _b '	4.53; 4.28	¹³ C	70.9
H _a 'H _c '	1.89; 1.75	¹³ C	34.5	H _a 'H _c '	1.44	¹³ C	34.1
H _b 'H _c '	1.51; 1.42	¹³ C	26.5	H _b 'H _c '	1.29	¹³ C	23.2

Experimental aromatic ester end group signals			Theoretical aromatic ester end group signals				
CH ₂ '	4.32	CH ₂ '	60.6	CH ₂ '	4.29	CH ₂ '	60.9
CH ₂ '	1.33	CH ₂ '	14.2	CH ₂ '	1.33	CH ₂ '	14.1

Signal of ¹³C-NMR at 28.8 ppm is a multiplet from 28.9 to 28.7.
 The symbol (↘) and (↙) distinguish the two independent conformers of the repeating unit (later called gg and gt).
 The symbol (↘↙) is used for the aliphatic-side OH end group signals.

Both chiral polymers showed the same chemical shifts and identical H_c' : H_c ratios: 76:24. This ratio would let us quantify the proportion between the two helical states for each enantiomeric polymer.

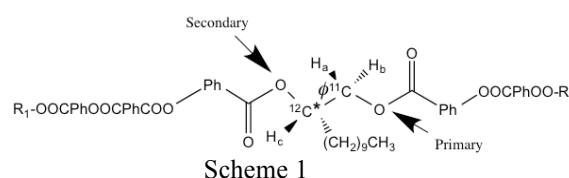
In the case of racemic PTOBDME, different H_c' : H_c proportions were observed depending on the polycondensation kinetics conditions, as will be shown later. As a consequence of this, its structure would consist of a mixture of four helical diastereomeric structures, two each present within R-PTOBDME and S-PTOBDME, in variable proportions.

Thus, we conclude that PTOBDME, obtained by polycondensation from TOBC and racemic DL:1,2-dodecanediol, was a stereoregular head-tail isotactic polymer. The regioselectivity of the head-tail reaction would be selected according to the larger reactivity of primary hydroxyl OH- groups than the secondary in the glycol, in agreement with Carothers [21], since structural and stereochemical factors will usually be more important factors than others, such as temperature, in bifunctional polycondensation reactions; these are almost completely determined by the nature of the reacting molecules.

The presence of a small amount of tail-head mesogen-spacer units in a majority head-tail polymer chain would generate multiple structures with different NMR spectra, not present in our case. Additionally a syndiotactic or atactic PTOBDME would also show different chemical shifts than those for R-PTOBDME and S-PTOBDME.

3.3. Conformational analysis

The structural fragment formed by a chiral secondary alcohol and a primary alcohol group (a beta-chiral 1,2-diol) is a particularly interesting class of diols present in many relevant natural products (such as sugars, nucleosides, glycerides) [22] and new designed chiral nanostructures from helical polymers and metallic salts [23].



In our case, the fragment in the spacer including the two alcohol groups is shown in Scheme 1. Details of molecular models for gg and gt conformers, in a dimer of PTOBDME, are shown in Fig. 8, the model is projected along the ¹¹C-¹²C bond, torsion ϕ , (perpendicular to the paper), with ¹²C having S absolute configuration (bonded to H_c) in yellow behind ¹¹C (bonded to H_a and H_b).

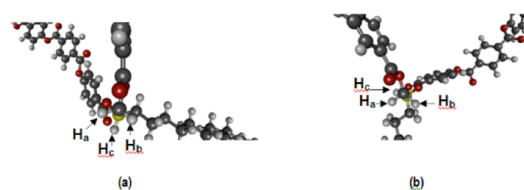


Figure 8. Molecular model detail of a PTOBDME dimer. View along ¹¹C-¹²C* bond (perpendicular to the paper), with (S)¹²C* (in yellow behind ¹¹C) for: (a) gg-conformer; (b) gt-conformer.

The vicinal coupling constants, ³J, between hydrogen H_c attached to asymmetric ¹²C* and the diastereotopic protons H_a, H_b bonded to carbon ¹¹C, were calculated by a Haasnoot-de Leeuw-Altona equation (chemical groups) [24] for the staggered conformers: gg and gt. They are shown in Fig. 9. According to this, the experimental values obtained for ³J_{Ha-Hc} (3.4 Hz) and for ³J_{Hb-Hc} (6.2 Hz) in system (), would indicate the preference of the gt conformer.

In system ('), the value for ³J_{Hc'-Ha'} (2.7 Hz), relatively low, would be interpreted as due to the preference of the gg conformer. Additionally protons H_a and H_b in system (') could be related with HproS and HproR, respectively, when the assymmetric ¹²C* was present in an S absolute configuration and the opposite when the absolute configuration was R. The same effect has also been reported for other related compounds [22]. In the case of system (') the overlapping of signal H_b' prevented the measurement of its coupling constant and also the assignment of H_a' and H_b' as HproS and HproR.

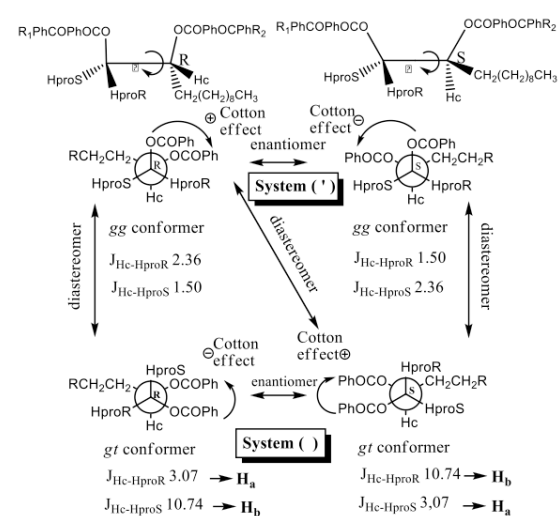


Figure 9. Calculated vicinal coupling constant of staggered conformations *gt* and *gg*, through the ^{11}C - $^{12}\text{C}^*$ bond (torsion ϕ) with R and S absolute configurations of carbon atom $^{12}\text{C}^*$. Relationship between helical conformations *gg* and *gt* and the sign of the Cotton effect produced are indicated.

The preference between *gg* and *gt* conformer was also related with the Cotton effect and the sign of helicity [25]. In the case of $^{12}\text{C}^*$ with an S absolute configuration, the sign of helicity and the Cotton effect were positive for *gt* conformation and negative for *gg* conformer and the opposite for R configuration.

The conformational analysis was corroborated with experimental results from NMR conventional techniques: 1D-selective NOESY, 1D-selective ROESY, NOSEY-2D and ROESY-2D. From a qualitative point of view, the most remarkable thing was the different behaviour between *gg* and *gt* conformers in the NOESY experiment, shown in Fig.10. While in *gg*, all NOE signals were positive (red), in *gt* there were positive signals for aromatic protons and negative signals (blue) for the aliphatic hydrogen atoms. The polymer molecular structure, with rigid aromatic rings linked by ester groups along the backbone and flexible aliphatic side chains, could explain this observation. Positive NOE are related with the more rigid aromatic zones and negative values with flexible chains.

^1H -NMR of PTOBDME was also obtained at 80°C; there was no change in size, shape and chemical shift of the signals for the *gg* and *gt* conformers. This indicates temperature would not affect equilibrium between the *gg* and *gt* conformers.

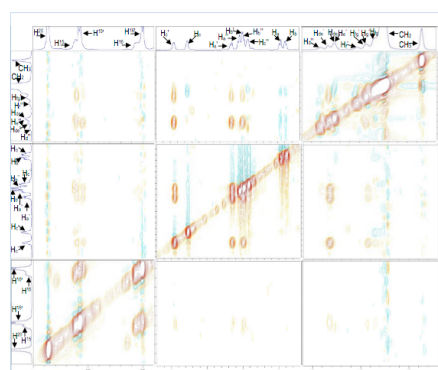


Figure 10. NOESY-2D Spectrum of R-PTOBDME. Positive NOE signals are in red, negative in blue.

3.4. Experimental molecular models

The Isolation Spin Pair Approach (ISPA) [26] was used to calculate inter-proton H-H distances (Å) between nuclei X and Y, considering the NOESY and ROESY signals intensities (%), according to equation $H_x-H_y = (H-H)_{ref} * [(\eta_{ref} / \eta_{xy})]^{(1/6)}$ (1), where η_{xy} is the intensity of the NOE for a given proton pair X and Y, H_x-H_y is the corresponding interproton distance, η_{ref} , and $(H-H)_{ref}$ are reference values for a single chosen NOE for which the interproton distance is assumed based on geometric constraint. The results, shown in Table 2, confirmed the presence of two helical conformers *gt* and *gg* observed in the scalar coupling and the preference of *gg* conformer in the systems ('), and *gt* in system without apostrophe.

Table 2. Interprotonic distances (Å) between nuclei X and Y calculated by ISPA from NOESY and ROESY spectral data, according to equation: $H_x-H_y = (H-H)_{ref} * [(\eta_{ref} / \eta_{xy})]^{(1/6)}$ (1).

		<i>gt</i> conformer				<i>gg</i> conformer							
H_c (5.25)	H_a (3.94)	Int(%)	d(Å)	H_b (3.88)	Int(%)	d(Å)	H_d, H_e (1.75)	Int(%)	d(Å)	H_f, H_g (1.33)	Int(%)	d(Å)	^{13}H (8.05)
		2.17	2.25	1.63	2.36	3.05	2.39	1.66	2.64	0.36	3.40		
H_c' (5.45)	H_a' (4.64)	Int(%)	d(Å)	H_b' (4.48)	Int(%)	d(Å)	H_d', H_e' (1.81)	Int(%)	d(Å)	H_f', H_g' (1.42)	Int(%)	d(Å)	^{13}H (8.13)
		13.23	2.25	12.23	2.28	13.60	2.52	3.12	3.20	2.10	3.42		

According to the experimental data, a polymer molecular model could be built for each conformer. In Fig. 11, two diastereomeric helical chains are shown, with an S absolute configuration of the asymmetric carbon ^{12}C , and with opposite screw sense. These models would explain the main features observed for PTOBDME, R-PTOBDME and S-PTOBDME. The combination of two diastereomeric helices with opposite screw sense with independent NMR signals and one asymmetric carbon atom per monomer, would result in two conformers for each enantiomer.

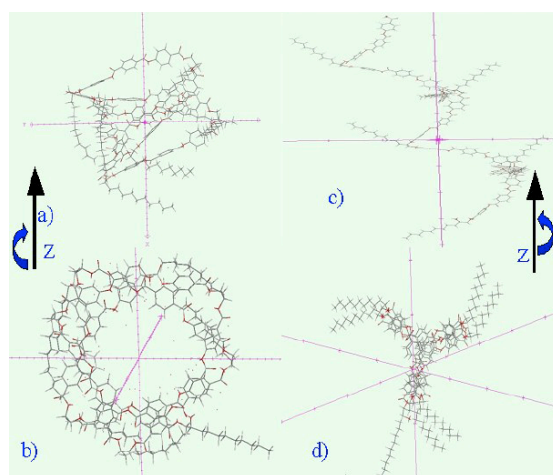


Figure 11. a) Lateral view of poly-S-PTOBDME *gg* conformer along Z axis and b) Cross Section; c) Lateral view of poly-S-PTOBDME *gt* conformer along Z and d) Cross Section.

One of the main structural differences between the conformers is the different position of the lateral chain with respect to the polymer main chain. In the *gg* conformer it is located among the benzoyl groups, Fig. 11(a) and Fig. 11(b) with the result its mobility is much more restricted, in agreement with the positive NOE values, than in the case of the *gt* conformer. The latter has a negative NOE with the side chains placed outside the benzoyl groups, Fig. 11(c) and Fig. 11(d) with a higher mobility.

In the case of chiral polymers R-PTOBDME and S-PTOBDME the optical activity would depend on the ratio between the two conformers with opposite helical sense and on the concentration of asymmetric carbon atoms. In the case of PTOBDME obtained from the racemic glycol its optical activity will depend on the relative amounts of the four diastereomers present, obtained by the combination of the two screw sense helices and the two absolute configurations of the asymmetric carbon atom.

3.5. Reaction kinetics study and their relationship with chirality.

In order to delve into the polycondensation mechanism of PTOBDME between equimolar quantities of TOBC and racemic R-S 1,2-dodecanediol, different kinetics conditions, summarized in Table 3, were utilized.

For the polycondensation of R-PTOBDME and S-PTOBDME the conditions used were: time of reaction 360 minutes, stirring rate 750 rpm, time of residence in toluene 1440 minutes and temperature 200°C in nitrogen atmosphere.

The yield of the polycondensation reaction is indicated for PTOBDME first fraction after different times of reaction: 60, 120, 180, 240, 360, 600 and 1440 min. The second and third fractions were obtained from the solvent recovered after the first

and second polymer precipitate fractions, respectively, had been removed. The results indicated that the yield of the first fraction decreased with increasing reaction time from 120 to 180, 240 and 360 min. It was also observed that the second and third fractions yields were considerably lower than the first fractions one. For each time of reaction, the total yields of precipitated fractions did not increase after 120 minutes; instead it decreased. The reaction seemed to be complete at this time. The time at which the second fraction precipitated increased with time of polycondensation reaction. Stronger stirring during polycondensation led to a better yield.

Table 3. Effect of the different reaction conditions on the polycondensation mechanism between TOBC and racemic D-L-1,2 dodecanediol, and their relationship with *gg* and *gt* diastereomeric helical structures observed by NMR.

Time of Reaction	Yield % first fraction	$gt/gg+gt$ (%)*	Yield % second fraction	$gt/gg+gt$ (%)*	Yield % third fraction	$gt/gg+gt$ (%)*	Stirring rate (rpm)	Time of residence in toluene	Time of second fraction precipitation	Time of third fraction precipitation
60 min		34.2					750	1440 min		
120 min	49.85	58.3	3.93	67.6	1.8	72.8	1000	1440 min	2 weeks	8 months and 2 weeks
180 min	35.74	73.6	6.6	85.2			1000	60 min	3 weeks	
240 min	29.54	57.4	1.41	61.2			750	1440 min**	2 months	
360 min	19.7	31.0		69.8			750	1440 min**		
600 min	50.07							1440 min		7 months
1440 min	14.73		2.36							

* Proportion between *gt* and *gg*, represented as ($gt/gg+gt$) (%), was calculated by the $H_c/(H_c+H_g)$ quotient, where H_c and H_g were measured by the integration of their 1H -NMR signals.

** After 240 and 360 minutes of reaction, PTOBDME was decanted in toluene for 60 minutes and filtered but it did not precipitate. After 1440 minutes it could be separated by filtration.

The time of residence in toluene of the polycondensation products poured from the reactor and stirred at room temperature was also considered. A shorter period of residence in toluene seemed to favour a higher yield of the second fraction.

The structure of the different PTOBDME fractions obtained by variation of the kinetics conditions were studied by NMR. They presented the same chemical shifts values. However differences in the relative signals integration were observed, interpreted as due to the different proportions between *gg* and *gt* helical conformation in each polymer, expressed as ($gt/gg+gt$) (%) in Table 3.

The helical conformation *gt* was mainly attained in the first fraction of PTOBDME after 120, 180 and 240 minutes of reaction, the last case in smaller proportion. Second fractions were always obtained with higher *chiral excess* than in the first fraction, being even higher in the third fraction, after 120 minutes of reaction.

The second fraction obtained after 180 minutes of polycondensation reaction, and decanted in toluene for 60 min, exhibited the highest *gt* content in the studied times. The optical behaviour of this polymer will be analyzed later in Table 4, compared to those polymerized for 120 and 360 min.

Helical *gg* conformer was observed primarily after polycondensation for 60 minutes and 360 minutes of reaction.

An explanation for these results could be found in the distinct PTOBDME species formed through the reaction course, in terms of a step-growth

polymerization, in which bi-functional monomers react to first form dimers, then trimers, longer oligomers and eventually long chain polymers [21]. The polymer chains would grow while diminishing their reactivity, reaching a maximum polymerization degree. After this point a *de*-polymerization process could begin to compete. Maximum yield would be attained when the concentration of larger polymer chains was high enough. Further reaction course would probably increase the number of shorter polymer chains by the *de*-polymerization process. Once the first fraction is removed, shorter polymer chains, much more reactive than intermediate ones, would still grow until chains were again large enough and the second fraction precipitates. In the case of R-PTOBDME and S-PTOBDME, the polycondensation with enantiomerically pure diols for 360 minutes showed a 24:76 *gt:gg* ratio, similar to the reaction with racemic starting materials, under the same kinetics conditions, for the first fraction, see Table 3.

3.6. NMR diffusion studies.

Diffusion ordered spectroscopy (DOSY) [27], [28], provided a method to evaluate molecular size variation of polymers by measurement of their diffusion coefficients (Δ), in DMSO- d_6 , in the case of R-PTOBDME, and PTOBDME (after 300 minutes of reaction). Two sets of signal were distinguished for R-PTOBDME: H_c' , H_a' and H_d' , interpreted as due to the *gg* conformer with $\log\Delta = -9.85$ and H_c , H_a , H_b and H_d , due to the *gt* conformer, with $\log\Delta = -9.78$, (the overlapping of the rest of signals led to an expected displacement and distortion of their peaks). However, the integration of all the signals resulted in a value of $\log\Delta = -9.78$ in spite of a higher proportion of the *gg* conformer. PTOBDME had slightly different values of $\log\Delta$; for *gg* -9.82 and for *gt* -9.77 , while the average $\log\Delta$ of all the signals was -9.75 . The slight difference between diffusion coefficients of *gg* and *gt* conformers could be explained in terms of their different flexibility also observed previously by NOE. Nevertheless, R-PTOBDME and PTOBDME presented a very similar $\log\Delta$, which indicated a similar polymerization degree, despite the different reaction kinetics conditions.

3.7. Optical activity.

Optical activity was evaluated for diols R(+)-1,2-dodecanediol and S(-)-1,2-dodecanediol and for the chiral polymers R-PTOBDME and S-PTOBDME, by measuring their ORD values (α). These values are given in Table 4, expressed as Molar Optical Rotation $[\Phi] = [\alpha] M/100$, M being the molecular weight of the polymer repeating unit, and shown in Fig. 12. They are compared with *racemic* PTOBDME polycondensed for three different times

of reaction: 120, 180 and 360 min., with second fractions containing higher *gt* diastereomer excess, 67.6%, 85.2% and 69.8%, respectively, as listed in Table 3.

The molar optical rotation of the chiral diols: R(+) and S(-)-1,2 dodecanediol, showed the expected positive and negative values respectively, for the studied wavelengths. Surprisingly, the sign of the diol changed when it was transformed into the polyester, R-PTOBDME and S-PTOBDME exhibiting negative and positive $[\Phi]$ values, respectively, for the studied wavelengths. Their absolute values were higher than those of the corresponding diol. A similar increase was also observed in a helical polyester previously reported [29, 30], where TOBC was polycondensed with optically active (S,S) dipropylene glycol, while it was not observed in polyesters with random coil structure [31]. The inversion of $[\Phi]$ sign in polymers with respect to enantiomerically pure monomers is not very common but it has been documented in other helical polymers [32, 33].

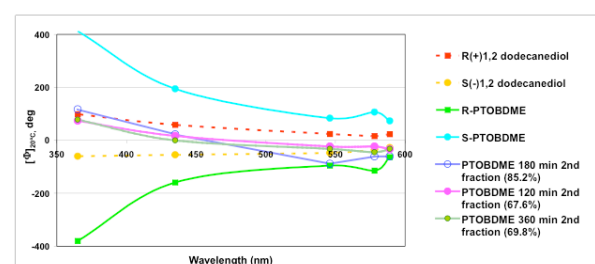


Figure 12. Molar Optical Rotation $[\Phi]$ of R(+)-1,2 dodecanediol; S(-)-1,2 dodecanediol; Polyesters R-PTOBDME, S-PTOBDME and several fractions of *racemic* PTOBDME, synthesized from *racemic* R,S-1,2 dodecanediol, obtained under different conditions, with helical conformation *gg* or *gt*, expressed as ratio *gt/gg+gt* (%) in Table 3.

Table 4. Experimental ORD values of R(+)-1,2-dodecanediol, S(-)-1,2-dodecanediol, R-PTOBDME, S-PTOBDME and *racemic* PTOBDME.

Wave-length (nm)	$[\Phi]_{DMSO}^{DOL}$ R(+)-1,2 dodecanediol 0.2gr/100ml in DMSO	$[\Phi]_{DMSO}^{DOL}$ S(-)-1,2 dodecanediol 0.2gr/100ml in DMSO	$[\Phi]_{DMSO}^{POLY}$ R-PTOBDME 0.28gr/100ml in DMSO	$[\Phi]_{DMSO}^{POLY}$ S-PTOBDME 0.26gr/100ml in DMSO	$[\Phi]_{DMSO}^{POLY}$ PTOBDME 180 min 2 nd fraction (85.2%) 0.1 gr/100ml in DMSO	$[\Phi]_{DMSO}^{POLY}$ PTOBDME 120 min 2 nd fraction (67.6%) 0.17 gr/100ml in DMSO	$[\Phi]_{DMSO}^{POLY}$ PTOBDME 360 min 2 nd fraction (69.8%) 0.14gr/100ml in DMSO
λ_{obs} 589	+23.1	-27.4	-63.5	+73.2	-61.2	-33.7	-32.6
λ_{obs} 578	+16.1	-35.5	-114.4	+106.4	-61.2	-23.5	-45.2
λ_{obs} 546	+24.1	-47.7	-95.5	+83.5	-88.7	-23.5	-32.6
λ_{obs} 435	+58.3	-54.9	-159.0	+194.5	+22.3	+16.6	0
λ_{obs} 365	+98.5	-60.6	-379.8	+411.8	+116.7	+73.8	+77.8

The $[\Phi]$ pattern of PTOBDME, polycondensed for 180 min from *racemic* R-S-1,2 dodecanediol, with the more enriched *gt* fraction, 85.2%, showed a behaviour parallel to the chiral polyester S-PTOBDME but with lower absolute $[\Phi]$ values, changing from positive sign at 365 and 435 nm, to zero at about 460 nm, and then to negative values at 546, 574 and 589 nm.

For the PTOBDME less in enriched fractions (67.6 and 69.8%), their absolute $[\Phi]$ values decreased with respect to the 85% *gt* polymer, both in the positive

and negative range, their values approaching towards that of R-PTOBDME.

In general the absolute values of $[\Phi]$ pattern in the *racemic* PTOBDME, increased with the diastereomeric excess in the polymer, either *gg* or *gt*, independently of which one was the main conformation.

The differences in $[\Phi]$ patterns between *racemic* PTOBDME, and chiral diols and R-PTOBDME and S-PTOBDME let us estimate the composition of the *racemic* PTOBDME. If chirality had only been caused by an enantiomeric excess of the R or S asymmetric carbon atom $^{12}\text{C}^*$, the $[\Phi]$ pattern of PTOBDME would be similar to those of the chiral diols, with an additional contribution due to a helical sense excess of diastereoisomers; the sum of the two contributions would generate a pattern similar to R-PTOBDME or S-PTOBDME.

An explanation for the ORD pattern of *racemic* PTOBDME, could be the preferable kinetic resolution of a diastereoisomer, such as *Sgt*, in a higher concentration with respect to the other three possible, hence approaching the S-PTOBDME pattern, while the R/S ratio of asymmetric carbon atoms remained 50:50. With decreasing *gt/gg* ratio, the $[\Phi]$ pattern would approach that of R-PTOBDME, due to the contribution of *Rgt* and *Rgg*. This could be the explanation of the origin of the unexpected chirality.

With these results we expect to contribute to clarify the helical sense and conformation of macromolecules during the synthetic process of cholesteric liquid-crystal polymer PTOBDME, based on their kinetics and optical activity characterization, key to understand their potential optoelectronic properties. Further study needs to be performed on the optoelectronic application of this cholesteric liquid crystal polymer, since a high interest is devoted at present in this field [34-42].

CONCLUSION

PTOBDME was synthesized by a polycondensation reaction as a chiral cholesteric liquid crystal polymer, starting from *racemic* raw materials. The study of the reaction kinetics, performed to understand the cause of the unexpected chirality, established some features of the polycondensation mechanism. Optimum yield was obtained after 120 minutes of polycondensation reaction, with 1000 rpm stirring rate and 1440 minutes time of subsequent residence in toluene. A second fraction precipitated two weeks later from the mother liquor had a higher diastereomeric excess (67.6%) and higher optical activity than the first polymer fraction. The yield of the second fraction was larger when the time of residence in toluene was 60 minutes. After eight months and two weeks a third fraction precipitated with 72.8% chiral excess.

The structure of *racemic* PTOBDME was analysed in solution by conventional NMR techniques, and compared with those of R-PTOBDME and S-PTOBDME obtained by starting with R(+)-1,2 and S(-)-1,2-dodecanediol, respectively. *Racemic* PTOBDME, R-PTOBDME and S-PTOBDME had the same stereoregular head-tail, isotactic polymeric structure formed by two diastereomeric helical conformations, related with the two possible types of staggered conformers of torsion ϕ (*gg* and *gt*) along the copolymer backbone, responsible for the two different independent set of signals observed by NMR for each enantiomer R-R-R-R and S-S-S-S. The regioselectivity of the head-tail reaction was explained by the higher reactivity of the primary hydroxyl than the secondary OH- group in the glycol. Experimental models were given by calculating interprotonic distances with the Isolation Spin Pair Approach (ISPA) from the NMR signals intensities.

The main difference between the molecular models of the *gg* and *gt* diastereomeric helical conformations was the different position of the lateral chains with respect to the polymer main chain. In the *gg* conformer it is located among the benzoyl groups with the result its mobility is much more restricted than in the case of the *gt* conformer where the side chains are placed outside the benzoyl groups with a higher mobility; NOESY experiment supported these molecular models; while in *gg*, all the NOE signals were positive red, related with the more rigid aromatic zones, in *gt* there were positive red signals for aromatic protons and negative blue signals for the aliphatic hydrogen atoms, related with flexible chains.

DOSY experiments confirmed the independence and similar polymerization degree between *gg* ($\log\Delta = -9.82$) and *gt* ($\log\Delta = -9.77$) diastereomers, they having very similar but not equal diffusion coefficient values. Their slight difference could be explained as due to the greater flexibility of the lateral hydrophobic chains in the *gt* conformer, in agreement with NOESY results.

Chirality in *racemic* PTOBDME is proposed to be due to the kinetic resolution of a preferable helical diastereomer, such as *Sgt*, with respect to the possible four forms, approaching the $[\Phi]$ S-PTOBDME pattern, while the R/S ratio of asymmetric carbon atoms remained 50:50.

Molar optical rotation $[\Phi]$ patterns of R(+) and S(-)-1,2 dodecanediol changed their sign when they were transformed into the respective polyesters R(-) PTOBDME and S(+) PTOBDME. In addition, an effect of chiral amplification was observed in both polymers by screw sense excess.

The $[\Phi]$ pattern of *racemic* PTOBDME, polycondensed for 180 min from *racemic* R-S-1,2 dodecanediol, obtained from the second fraction

with the more enriched *gt* fraction (85.2%), showed a behaviour parallel to chiral polyester S-PTOBDME but with lower absolute $[\Phi]$ values, changing from positive sign to negative. With decreasing *gt* diastereomer excess, the PTOBDME less enriched fractions (67.6 and 69.8%), had lower absolute $[\Phi]$ values with respect to the 85% *gt* polymer, both in the positive and negative range, approaching in tendency towards that of R-PTOBDME.

The results given here are a contribution to clarify the helical sense and conformation of macromolecules during the synthetic process of cholesteric liquid-crystal polymer PTOBDME, based on their kinetics and optical activity characterization, key to understand their potential optoelectronic properties. Further study needs to be performed on the optoelectronic application of this cholesteric liquid crystal polymer, since a high interest is devoted at present in this field.

Acknowledgement

The authors thank Mr.J Guisandez for his help in the laboratory and Prof. J. Jimenez Barbero for his support with the NMR measurements.

We also thank the CSIC (MEC) for financial support with project PTR1995-0760-OP.

REFERENCES

- [1.] O Vogl, L S Corley, W J Harris, G D Jaycox and J Zhang: Optical activity based on macromolecular asymmetry. *Makromol.Chem.,Suppl.* 1985, **13**:1-12.
- [2.] H Ringsdorf, B Schlarb, J Venzmer: Molecular architecture and function of polymeric oriented systems: models for the study of organization, surface recognition, and dynamics of biomembrane. *Ang. Chem. Int. Ed. Engl.* 1988, **27**, 113.
- [3.] M Pérez-Méndez, C Marco Rocha, Process for obtaining cholesteric liquid crystals by stereoselective recrystallization. Patents EP1004650-A, WO9831771-A, WO9831771-A1, AU9854863-A, ES2125818-A1, ES2125818-B1, EP1004650-A1, US6165382-A, MX9906732-A1, JP2001513827-W, AU739076-B, EP1004650-B1, DE69824182-E.
- [4.] A Y Bilibin, A V Ten'kovtsev, O N Piraner, S S Skorokhodov: Synthesis of high-molecular weight liquid crystal polyesters based on a polycondensation mesogenic monomer. *Polym. Sci. U.S.S.R.* 1984, **26**, n° 12: 2882-2890.
- [5.] S S Skorokhodov, A Y Bilibin: Rational path of the synthesis of liquid-crystalline high-molecular-weight polyesters and their properties in solution. *Makromol. Chem. Makromol. Symp.* 1989, **26**: 9-23.
- [6.] J Fayos, S Sanchez-Cortes, C Marco, M Perez-Mendez: Conformational analysis and molecular modeling of cholesteric liquid crystal polyesters based on XRD, Raman, and transition thermal analysis. *J. Macromol. Sci., Part B,Phys.* 2001, **40**: 553-576.
- [7.] M Pérez-Méndez, C Marco Rocha: New Synthesis, Thermal Properties and Texture of Cholesteric Poly[oxy(1,2-butene)oxycarbonyl-1,4-Phenyleneoxycarbonyl-1,4-phenylene carbonyloxy -1,4-phenylenecarbonyl], PTOBEE. *Acta Polym.* 1997, **48**: 502-506.
- [8.] M Perez-Mendez, R Marsal, L Garrido, M Martin-Pastor: Self-Association and Stereoselectivity in a Chiral Liquid-Crystal Colesteric Polymer Formed under Achiral Conditions. *Macromolecules* 2003, **36**: 8049-8055.
- [9.] M Pérez-Méndez, J Fayos, C R Mateo: *Advances in Biochirality, Chapter 24*: Self-assembly of cholesteric liquid crystal polyesters and their stereoselective interaction with liposomes of DMPC, Elsevier Science S. A. 1999: 325-334.
- [10.] M Perez-Mendez, R Marsal, S Sanchez-Cortes: Adsorption of a Cholesteric Liquid-crystal Polyester on Silver and Gold Nanoparticles and Films Studied by Surface-Enhanced Raman Scattering. *Appl. Spectros.* 2004, **58**: 562- 569.
- [11.] M Perez-Mendez, J Fayos, G P Blanch, S Sánchez Cortés: *Encyclopedia of Nanoscience and Nanotechnology, Biofunctionalization of Cholesteric Liquid-Crystal Helical Polymers. Nanocarriers*, 11: 547-580, Edited by H. S. Nalwa, ACS. American Scientific Publishers USA **2011**. ISBN: 1-58883-160-4 .
- [12.] J C Cobas, F J Sardina: Nuclear magnetic resonance data processing: MestRe-C, a software package for desktop computers. *Concepts Magn. Reson.* 2003, **19A**: 80-96.
- [13.] F Iwasaki, T Maki, O Onomura, W Nakashima, Y Matsumura: Chemo- and stereoselective monobenzoylation of 1,2-diols catalyzed by organotin compounds. *J. Org. Chem.* 2000, **65**: 996-1002.
- [14.] A Khalafi-Nezhad, M N Soltani Rad, A Khoshnood: An Efficient Method for the Chemoselective Preparation of Benzoylated 1,2-Diols from Epoxides. *Synthesis* 2003, **16**: 2552-2558.
- [15.] S Caddick, A J McCarrol, D A Sandman: A convenient and practical method for the

- selective benzylation of primary hydroxyl groups using microwave heating. *Tetrahedron* 2001, 57: 6305-6310.
- [16.] K Ute, K Hirose, H Kashimoto, K Hatada, O Vogl: Haloaldehyde polymers. 51. Helix-sense reversal of isotactic chloral oligomers in solution. *J. Am. Chem. Soc.* 1991, 113: 6305- 6306.
- [17.] K Ute, K Oka, Y Okamoto, K Hatada, F Xi, O Vogl: Haloaldehyde polymers LIII. Optical resolution of purely isotactic oligomers of chloral: optical activity of the chloral oligomers assuming one-handed helical conformation in solution. *Polym. J.* 1991, 23: 1419-1424.
- [18.] K Ute, K Hirose, H Kashimoto, H Nakayama, K Hatada, O Vogl: Helix-Inversion Equilibrium of Isotactic Chloral Oligomers in Solution. *Polym. J.* 1993, 25, N° 11: 1175- 1186.
- [19.] J Tabei, M Shiotsuki, T Sato, F Anda, T Masuda: Control of Helix Sense by Composition of Chiral-Achiral Copolymers of N- Propargylbenzamides. *Chem. Eur. J.* 2005, 11: 3591-3598.
- [20.] E Yashima, K Maeda, T Nishimura: Detection and amplification of chirality by helical polymers. *Chem. Eur. J.* 2004, 10: 42-51.
- [21.] W. H Carothers: Studies on polymerization and ring formation. i. an introduction to the general theory of condensation polymers. *J. Am. Chem. Soc.* 1929, 51 (8): 2548.
- [22.] F Freire, J M Seco, E Quiñoá, R Riguera: The prediction of the absolute stereochemistry of primary and secondary 1,2-diols by ¹H NMR spectroscopy: Principles and applications. *Chem. Eur.J.* 2005, 11: 5509-5522.
- [23.] S Arias, F Freire, E Quiñoá, R Riguera: Nanospheres, Nanotubes, Toroids, and Gels with Controlled Macroscopic Chirality. *Angew. Chem. Int. Edition* 2014, 53, Issue 50:13720-13724.
- [24.] C A G Haasnoot, F A A M Deleuw, C Altona: The relationship between proton-proton NMR coupling constants and substituent electronegativities-I. *Tetrahedron* 1980, 36: 2783-2792.
- [25.] H Uzawa, Y Nishida, H Ohru, H Meguro: Application of the dibenzoate chirality method to determine the absolute configuration of glycerols and related acyclic alcohols. *J. Org. Chem.* 1990, 55(1): 116-122.
- [26.] D Neuhaus, M P Williamson: The Nuclear Overhauser Effect in Structural and conformational Analysis, 2nd edition, Wiley-VCH, Weinheim 2000.
- [27.] A Chen, D Wu, C S Jr Johnson: Determination of molecular weight distributions for polymers by diffusion-ordered NMR. *J. Am. Chem. Soc.* 1995, 117: 7965- 7970.
- [28.] P Groves, M O Rasmussen, M D Molero, E Samain, F J Cañada, H Driguez, J Jimenez-Barbero: Diffusion ordered spectroscopy as a complement to size exclusion chromatography in oligosaccharide analysis. *Glycobiology* 2004, 14: 451-456.
- [29.] E Chiellini, G Galli, S Carrozzino: Chiral Liquid Crystal Polymers. 10. Thermotropic mesomorphism in chiral isomeric polyesters. *Macromolecules* 1990, 23: 2106-2112.
- [30.] K Toyofuku, Md A Alam, A Tsuda, N Fujita, S Sakamoto, K Yamaguchi, T Aida: Amplified chiral transformation through helical assembly. *Angew. Chem. Int. Ed.* 2007, 46: 6476-6480.
- [31.] E Chiellini, G Galli: Chiral liquid crystal polymers, 4. Chiroptical properties of thermotropic polyesters in dilute solution. *Makromol. Chem. Rapid. Commun.* 1983, 4(5): 285-289.
- [32.] Y. Okamoto, M. Nishikawa, T. Nakano, E. Yashima, K. Hatada, Induction of a single-handed helical conformation through radical polymerization of optically active phenyl-2-pyridyl-o-tolylmethyl methacrylate. *Macromolecules* 1995, 28, 5135-5138.
- [33.] S Ohkawa, F Yang, K Kawabata, H Goto: Synthesis of polymers from chiral monomers in chiral liquid crystals. *J. Appl. Polym. Sci.* 2012, DOI: 10.1002/APP.38561, 1-6, first published on line: 30 sep 2012.
- [34.] a) G Tian, Y Lu, B M Novak: Helix-Sense Selective Polymerization of Carbodiimides: Building Permanently Optically Active Polymers from Achiral Monomers. *J. Am. Chem. Soc.* 2004, 126: 4082-4083.
- [35.] D Pijper, B L Feringa: Molecular Transmission: Controlling the twist sense of a helical polymer with a single light-driven molecular motor. *Angew. Chem. Int. Ed.* 2007, 46: 3693-3696.
- [36.] K Maeda, K Morioka, E Yashima: Synthesis and chirality sensing properties of Poly[(phenyleneethynylene)-*alt*-(carboxybiphenyleneethynylene)]s. *Macromolecules* 2007, 40: 1349-1352.
- [37.] T Kawauchi, A Kitaura, J Kumaki, H Kusanagi, E Yashima: Helix-sense-controlled synthesis of optically active Poly(methyl methacrylate) stereocomplexes. *J. Am. Chem. Soc.* 2008, 130: 11889-11891.

- [38.] J-H Liu; F-M Hsieh: Synthesis and characterization of pitch tunable cholesteric liquid crystalline polymers. *Proc. SPIE* 2009, **7232**, Emerging Liquid Crystal Technologies IV, 72320C. doi: 10.1117/12.813596.
- [39.] I Shinichi, K P Devproshad, M A Salam, N Haraguchi: Main-chain ionic chiral polymers: Synthesis of optically active quaternary ammonium sulfonate polymers and their application in asymmetric catalysis. *J. Am. Chem. Soc.* 2010, 132(9): 2864–2865.
- [40.] J Zhou, G Ke, B Wang, H Chen, G Chen, R Li: Liquid crystal optically variable device with continuously distributed colors, *Opt. Eng.* 2011 **50(8)**, 081203. doi:10.1117/1.3565042
- [41.] A T Petkoska, S D Jacobs: The Manufacture, Characterization and Manipulation of Polymer Cholesteric Liquid Crystal Flakes and Their Possible Applications. *J. Mater. Sci. Eng. A 2* 2012 (2), 137–151.
- [42.] M Mohammadimasoudi, J Beeckman, K Neyts: Effect of UV curing conditions on polymerized tunable chiral nematic liquid crystals. *Proceeding of SPIE* 2014, **9182**, 91821A- 1- 91821A-7.

Table 1. ^1H and ^{13}C -NMR Chemical Shifts (ppm) observed and calculated for the Chiral Polyester PTOBDME obtained from racemic 1,2 dodecanediol

Set of signal of gg helical conformer (↘)				Set of signal of gt helical conformer (↗)				Calculated Chemical Shifts	
Atom	^1H ppm	Atom	^{13}C ppm	Atom	^1H ppm	Atom	^{13}C ppm	^1H ppm	^{13}C ppm
^{20}H	8.36	^{20}C	130.4	^{20}H	8.36	^{20}C	130.4	8.04	130.2
		^{19}C	133.2			^{19}C	133.2		135.5
		^{18}C	163.5			^{18}C	163.4		165.2
		^{17}C	153.9			^{17}C	154.4		155.7
^{16}H	7.50;7.48	^{16}C	122.2	^{16}H	7.57;7.55	^{16}C	122.5	7.26	121.5
^{15}H	8.07;8.05	^{15}C	131.0	^{15}H	8.13;8.11	^{15}C	131.0	8.13;8.11	130.3
		^{14}C	128.7			^{14}C	127.3		127.0
		^{13}C	166.6			^{13}C	164.5		166.0
H_c^*	5.45	^{12}C	72.6	H_c	5.26	^{12}C	73.4	4.55	70.4
H_a^*H_b^*	4.64, 4.48	^{11}C	66.0	H_aH_b	3.94, 3.88	^{11}C	46.4	4.80,4.55	67.6
H_c^*H_d^*	1.81	^{10}C	30.3	H_cH_d	1.75	^{10}C	31.1	1.71	30.8
H_e^*H_f^*	1.42	^9C	24.5	H_eH_f	1.33	^9C	24.5	1.29	23.4
^{8a}H	1.22	^8C	28.9(m)*	^{8a}H	1.22	^8C	28.9(m)*	1.29	29.7
^{7a}H	1.22	^7C	28.9(m)*	^{7a}H	1.22	^7C	28.9(m)*	1.29	29.7
^{6a}H	1.22	^6C	28.8(m)*	^{6a}H	1.22	^6C	28.8(m)*	1.26	29.7
^{5a}H	1.22	^5C	28.7(m)*	^{5a}H	1.22	^5C	28.7(m)*	1.26	29.7
^{4a}H	1.22	^4C	28.4(m)*	^{4a}H	1.22	^4C	28.4(m)*	1.26	29.4
^{3a}H	1.22	^3C	31.3	^{3a}H	1.22	^3C	31.3	1.26	31.9
^{2a}H	1.22	^2C	22.1	^{2a}H	1.22	^2C	22.1	1.26	22.8
^{1a}H	0.84	^1C	14.0	^{1a}H	0.84	^1C	14.0	0.86	14.1
Experimental aliphatic end group signals				Theoretical aliphatic end group signals					
H_c^{**}	4.40	$^{12**}\text{C}$	60.4	H_c^{**}	3.81	$^{12**}\text{C}$			70.9
$\text{H}_a^{**}\text{H}_b^{**}$	4.48; 4.49	$^{11**}\text{C}$	67.8	$\text{H}_a^{**}\text{H}_b^{**}$	4.53; 4.28	$^{11**}\text{C}$			70.9
$\text{H}_c^{**}\text{H}_d^{**}$	1.89; 1.75	$^{10**}\text{C}$	34.5	$\text{H}_c^{**}\text{H}_d^{**}$	1.44	$^{10**}\text{C}$			34.1
$\text{H}_e^{**}\text{H}_f^{**}$	1.51; 1.42	$^9**\text{C}$	26.5	$\text{H}_e^{**}\text{H}_f^{**}$	1.29	$^9**\text{C}$			23.2
Experimental aromatic ester end group signals				Theoretical aromatic ester end group signals					
CH_2^*	4.32	CH_2^*	60.6	CH_2^*	4.29	CH_2^*			60.9
CH_3^{**}	1.33	CH_3^*	14.2	CH_3^{**}	1.33	CH_3^*			14.1

Signal of ^{13}C -NMR at 28.8 ppm is a multiplet from 28.9 to 28.7.

The symbol (↘) and (↗) distinguish the two independent conformers of the repeating unit (later called gg and gt).

The symbol (↘↘) is used for the aliphatic-side OH end group signals.

Table 2. Interprotonic distances (Å) between nuclei X and Y calculated by ISPA from NOESY and ROESY spectral data, according to equation: $H_x-H_y = (H-H)_{ref} * [(\eta_{ref} / \eta_{xy})]^{(1/6)}$ (1).

		<i>gt conformer</i>									
		H _a (3.94)		H _b (3.88)		H _d , H _e (1.75)		H _f , H _g (1.33)		¹⁵ H (8.05)	
		Int(%)	d(Å)	Int(%)	d(Å)	Int(%)	d(Å)	Int(%)	d(Å)	Int(%)	d(Å)
H _c (5.25)		2.17	2.25	1.63	2.36	3.05	2.39	1.66	2.64	0.36	3.40
		<i>gg conformer</i>									
		H _a ' (4.64)		H _b ' (4.48)		H _d ', H _e ' (1.81)		H _f ', H _g ' (1.42)		¹⁵ H (8.13)	
		Int(%)	d(Å)	Int(%)	d(Å)	Int(%)	d(Å)	Int(%)	d(Å)	Int(%)	d(Å)
H _c ' (5.45)		13.23	2.25	12.23	2.28	13.60	2.52	3.12	3.20	2.10	3.42

Table 3. Effect of the different reaction conditions on the polycondensation mechanism between TOBC and racemic D-L-1,2 dodecanediol, and their relationship with *gg* and *gt* diastereomeric helical structures observed by NMR.

Time of Reaction	Yield % first fraction	<i>gt/gg+gt</i> (%)*	Yield % second fraction	<i>gt/gg+gt</i> (%)*	Yield % third fraction	<i>gt/gg+gt</i> (%)*	Stirring rate (rpm)	Time of residence in toluene	Time of second fraction precipitation	Time of third fraction precipitation
60 min		34.2					750	1440 min		
120 min	49.85	58.3	3.93	67.6	1.8	72.8	1000	1440 min	2 weeks	8 months and 2 weeks
180 min	35.74	73.6	6.6	85.2			1000	60 min	3 weeks	
240 min	29.54	57.4	1.41	61.2			750	1440 min**	2 months	
360 min	19.7	31.0		69.8			750	1440 min**		
600 min	50.07		2.36					1440 min	7 months	
1440min	14.73									

* Proportion between *gt* and *gg*, represented as (*gt/gg+gt*) (%), was calculated by the H_c/(H_c+H_c') quotient, where H_c' and H_c were measured by the integration of their ¹H-NMR signals.

** After 240 and 360 minutes of reaction, PTOBDME was decanted in toluene for 60 minutes and filtered but it did not precipitate. After 1440 minutes it could be separated by filtration.

Table 4. Experimental ORD values of R(+)-1,2-dodecanediol, S(-)-1,2-dodecanediol, R-PTOBDME, S-PTOBDME and racemic PTOBDME.

Wave-length [nm]	$[\Phi]_{20^\circ C}$ R(+)-1,2 dodecanediol 0.2gr/100ml in DMSO	$[\Phi]_{20^\circ C}$ S(-)-1,2 dodecanediol 0.2gr/100ml in DMSO	$[\Phi]_{20^\circ C}$ R- PTOBDME 0.28gr/100ml in DMSO	$[\Phi]_{20^\circ C}$ S- PTOBDME 0.26gr/100ml in DMSO	$[\Phi]_{20^\circ C}$ PTOBDME 180 min 2 nd fraction (85.2%) 0.1 gr/100ml in DMSO	$[\Phi]_{20^\circ C}$ PTOBDME 120 min 2 nd fraction (67.6%) 0.17 gr/100ml in DMSO	$[\Phi]_{20^\circ C}$ PTOBDME 360 min 2 nd fraction (69.8%) 0.14gr/100ml in DMSO
λ_{Na} 589	+ 23.1	- 27.4	- 63.5	+ 73.2	- 61.2	- 33.7	- 32.6
λ_{Hg} 578	+ 16.1	- 35.5	- 114.4	+ 106.4	- 61.2	- 23.5	- 45.2
λ_{Hg} 546	+ 24.1	- 47.7	- 95.5	+ 83.5	- 88.7	- 23.5	- 32.6
λ_{Hg} 435	+ 58.3	- 54.9	- 159.0	+ 194.5	+ 22.3	+ 16.6	0
λ_{Hg} 365	+ 98.5	- 60.6	- 379.8	+ 411.8	+ 116.7	+ 73.8	+ 77.8